Learning by doing: seasonal and diurnal features of tropical precipitation in a global-coupled storm-resolving model

Hans Segura[1], Cathy Hohenegger[1], Christian Wengel[2], and Bjorn Stevens[1]

[1]Max Planck Institute for Meteorology
[2]Unknown

January 20, 2023

Abstract

Using the global and coupled ICON-Sapphire model with a grid spacing of \SI{5}{\kilo\meter}, we describe seasonal and diurnal features of the tropical rainbelt and assess the limits of ICON-Sapphire in representing tropical precipitation. Aside from the meridional migration, the tropical rainbelt exhibits a seasonal enlargement and a zonal migration. Surprisingly, ICON-Sapphire reproduces these characteristics with better performance over land than over ocean and with a very high degree of agreement to observations. ICON-Sapphire especially struggles in capturing the seasonal features of the tropical rainbelt over the oceans of the Eastern Hemisphere, an issue associated with a cold SST bias at the equator. ICON-Sapphire also shows that a perfect representation of the diurnal cycle of precipitation over land is not a requirement to capture the seasonal features of the rainbelt over land, while over the ocean, 5km is sufficient to adequately represent the diurnal cycle of precipitation.

Learning by doing: seasonal and diurnal features of tropical precipitation in a global-coupled storm-resolving model

H. Segura[1], C. Hohenegger[1], C. Wengel[1], B. Stevens[1]

[1]Max Planck Institute for Meteorology

Key Points:

- ICON in a global and coupled configuration at km-scale (ICON-S) simulates the characteristics of the diurnal cycle in the tropics.
- In one year of simulation, ICON-S reproduces the seasonal features of the tropical rainbelt over land with high agreement with observations.
- Biases in sea surface temperature explains the struggles of ICON-S in simulating the oceanic rainbelt of the Eastern Hemisphere.

Corresponding author: H. Segura, `hans.segura@mpimet.mpg.de`

Abstract

Using the global and coupled ICON-Sapphire model with a grid spacing of 5 km, we describe seasonal and diurnal features of the tropical rainbelt and assess the limits of ICON-Sapphire in representing tropical precipitation. Aside from the meridional migration, the tropical rainbelt exhibits a seasonal enlargement and a zonal migration. Surprisingly, ICON-Sapphire reproduces these characteristics with better performance over land than over ocean and with a very high degree of agreement to observations. ICON-Sapphire especially struggles in capturing the seasonal features of the tropical rainbelt over the oceans of the Eastern Hemisphere, an issue associated with a cold SST bias at the equator. ICON-Sapphire also shows that a perfect representation of the diurnal cycle of precipitation over land is not a requirement to capture the seasonal features of the rainbelt over land, while over the ocean, 5km is sufficient to adequately represent the diurnal cycle of precipitation.

Plain Language Summary

The success of storm resolving models (SRMs) by reproducing synoptic weather conditions motivated the scientific climate community to use them for climate studies. By explicitly solving the 3-D wind field, SRMs can capture the interaction of kilometer-scale processes with the large-scale flow, improving the representation of tropical precipitation compared to coarse-resolution models using convective parameterization. Tropical precipitation plays an important role in the vertical transport of energy, a key parameter in the understanding of future changes in the Earth's climate under the current global warming. By using ICON in a global and coupled configuration at 5km of resolution, we show that seasonal and diurnal features of the tropical rainbelt can be reproduced as the meridional and zonal migration and the diurnal cycle of precipitation. Furthermore, we identify seasonal changes in the structure of the rainbelt over the land, which is associated with monsoon seasons and that ICON can capture. The enlargement is also observed over the ocean. While ICON presents a double ITCZ bias in the Indo-Pacific region, our results open the possibility of using ICON to analyze the duration of monsoon seasons, along with the zonal migration and the enlargement of the rainbelt over the ocean.

1 Introduction

Storm-resolving models (SRMs) distinguish themselves from traditional climate models through their explicit representation of fluid dynamical processes on the scale of a few, to a few tens, of kilometers. Motions on these scales, referred to as the meso-beta scale, shape the dynamics of convective precipitation – one of the climate system's most important processes. Decades of experience with regional models designed to simulate processes on these scales (Baldauf et al., 2011; Done et al., 2004; Grell et al., 2000; Hohenegger et al., 2008; Prein et al., 2013), suggest that the emerging capability to also explicitly represent such processes on global domains (Dirmeyer et al., 2012; Miura, Satoh, Nasuno, et al., 2007; Miura, Satoh, Tomita, et al., 2007; Satoh et al., 2017; Stevens et al., 2020) will lead to more physical and more useful simulations of the Earth-system as a whole (Slingo et al., 2022).

The advantages of explicitly representing, rather than parameterizing, convection are manifold, uncontroversial and amply documented (Marsham et al., 2013; Satoh et al., 2019; Schär et al., 2020), justifying the excitement of using global SRMs (GSRMs) to represent the climate system. However, maximizing the potential of GSRMs will require effort. Some important climate processes remain unresolved at the kilometer scale, notably cloud mixing and cloud microphysical processes that structure non-precipitating convection (Mellado et al., 2018; Stevens et al., 1999). Moreover, in efforts to anticipate the insights that will be enabled by GSRMs, it is tempting to compromise resolution for throughput, with consequences for simulation fidelity. For instance, in our group most of our efforts have focused on a grid-scale of 5 km, often considered marginal to represent many convective scale processes. While the impact of such trade-offs has been demonstrated for case studies of isolated systems (Marsham et al., 2013; Pearson et al., 2014; Prein et al., 2013), their effects globally are far from clear. Beyond the question of trade-offs, a more fundamental question is how an improved representation of meso-beta scale processes influences air-sea coupling. This question, unlike over land, has been much less studied. Particularly in the tropics, where subtle changes in SST and small shifts in the wind can strongly influence convection.

These issues motivate the present study, which analyzes the behavior of the coupled system when allowing for an explicit, albeit coarse, representation of meso-beta scale processes for an entire annual cycle. The simulations are performed using the ICON model with a grid spacing of 5 km across all components (Hohenegger et al., 2022). These are, to our knowledge, the first simulations of their kind. This also means that the model system is still in an early stage of its development, leading to a greater potential for errors and imbalances. From this perspective, identifying what the simulations represent poorly helps target efforts to find implementation errors and to understand to what extent errors generalize. Together with an identification of what the simulations get right, even at their more marginal resolution, this allows a better assessment of the trade offs between resolution and throughput.

Specifically we investigate which aspects of the diurnal and, for the first time, the seasonal cycle of tropical precipitation are (or are not) reproduced by a 5 km mesh coupled GSRM. This focus was chosen because such cycles represent the leading mode of forced variability, and as such the dominant signal of the climatic response to forcing, of those processes that SRMs are expected to get right. Our analysis of the seasonal cycle goes beyond a simple bias analysis, to additionally describe the seasonal evolution of the tropical rainbelt using an object based analysis. This allows to explore the sensitivity of the annual cycle of tropical precipitation to developing SST biases (irrespective of their source) as these are expected to couple to planetary scale energy transports (Adam et al., 2016; Schneider et al., 2014) to which the convection may be sensitive. Our analysis of the diurnal cycle of precipitation serves as a reference point for the representation of small-scale processes, and allows to address the impact of the representation of this variability on the seasonal features of tropical rainbelts.

2 Methods

2.1 ICON-Sapphire

We analyze simulations from a new ICON configuration, called Sapphire (Hohenegger et al., 2022), or ICON-S. ICON-S targets the representation of kilometer-scale processes across all components of the Earth system. We analyze the G_AO_5 km simulation described by Hohenegger et al. (2022), which employs a grid spacing of 5 km and 90 vertical levels in the atmosphere, 128 levels in the ocean and five in the land. The simulation is started using the IFS analysis from January 20, 2020, and is run until February 28, 2021.

To compare the model with observation, precipitation in ICON-S is interpolated to a regular grid of 0.1°x 0.1°. To allow a spin-up of the smaller scales of motion, the first 11 days of the simulation are discarded. To analyze the seasonal cycle, monthly means are calculated from February 2020 to January 2021, and for the diurnal cycle analysis, hourly precipitation for February 2020 is used because the mechanisms related to this variability are the same throughout the year in the tropics.

2.2 GPM data

We use the IMERG V06 data set from January 2001 to January 2021 (Huffman et al., 2019) for comparison to the ICON-S simulations. The IMERG data set is downloaded from the Integrated Climate Data Center website (`https://www.cen.uni-hamburg.de/en/icdc/data/atmosphere/imerg-precipitation-amount.html`). The climatology of IMERG is computed from monthly mean data for the period between January 2001 to January 2021. The diurnal precipitation cycle from IMERG is analyzed for the same period (February 2020) as for ICON-S, using hourly data.

2.3 SAL method

To quantify and compare the seasonal evolution of the simulated tropical rainbelt with that inferred from observations, we make use of the SAL method (Wernli et al., 2008). The SAL method segments continuous grid cells where the value of precipitation is greater than a threshold. The resulting objects are then quantified in terms of their (S)structure, (A)amplitude, and (L)location. Precipitation objects are calculated for different regions within the tropics (30°S-30°N), making a distinction between ocean and land. The tropical rainbelt is defined as the precipitation object holding the largest area in each region. We are aware that by using this methodology, we can not properly characterize the finest structure of the tropical rainbelt, but as our objective is to analyze the seasonal changes and not the intraseasonal or day-to-day variations, we consider this approach valid. Moreover, the SAL method has proven useful in several past studies to analyze the Intertropical Convergence Zone (ITCZ) and monsoon regions (Hohenegger & Stevens, 2013; Siongco et al., 2015, 2017).

3 Tropical precipitation

3.1 The annual mean structure

Figure 1a shows that ICON-S can represent the annual mean structure of tropical precipitation. In particular the location of convective regions, enclosed by the quantile 80 (q80), in ICON-S is similar than in the climatology of IMERG, most notably in the regions between the central Pacific and western Africa. Discrepancies are largest in the vicinity of the maritime continent. This is evident when calculating the percentage of grid cells in ICON-S inside the q80 contour that matches IMERG, being higher in the Western Hemisphere (180° W-0° E), with values around 73 %, than in the Eastern hemisphere (47 %).

There are three biases that stand out, the double precipitation band in the Indo-Pacific region, the more zonally elongated Southern Pacific Convergence Zone, and the signature of a double ITCZ on the eastern Pacific. Moreover, a calculation of the index used by Samanta et al. (2019) to quantify the double ITCZ in the central Pacific gives a value of six (6). This is a similar value compared to CMIP5 and CMIP6 models, but three times more than in observational data sets (Fiedler et al., 2020). Because individual years in IMERG do not sample the extreme values found in this analysis, we interpret these features as biases in ICON-S. If such biases prove to be recalcitrant in SRMs, it suggests that their origin lies less in the representation of convection and more in how convection couples to subgrid-scale processes including those within the ocean.

The mean tropical precipitation in ICON-S is $3.7\,\mathrm{mm\,d^{-1}}$, $0.3\,\mathrm{mm\,d^{-1}}$ larger than for IMERG (Figure S1). Part of this might be due to satellite observations underestimating precipitation (Pfeifroth et al., 2013; Lu & Yong, 2018; Bulovic et al., 2020), but the ICON dynamics also leaks energy (Gassmann, 2013) in ways that cause the atmosphere to cool more than would be expected based on its radiative cooling, which would otherwise constrain the rate of precipitation. The bias is higher over the land ($0.5\,\mathrm{mm\,d^{-1}}$)

than over the ocean ($0.2\,\mathrm{mm\,d^{-1}}$). ICON-S can reproduce the partitioning of precipitation between land and ocean, which is close to one as documented by Hohenegger and Stevens (2022) using other observational datasets, a feature that models using parameterized convection are not able to capture (Hohenegger & Stevens, 2022).

3.2 Summer-winter amplitude and diurnal cycle

ICON-S also reproduces the pattern of the seasonal difference in precipitation between the austral and boreal summer observed in the climatology of IMERG (Figure 1b). Among the characteristics that ICON-S reproduces are the seasonal location of convective regions (marked by the value of $\pm\,3\,\mathrm{mm\,d^{-1}}$), the poleward extension of the convective regions over land and the Indo-Pacific warm pool in their respective summer season, and a wider convective region in the Northern than in the Southern Hemisphere over the eastern Pacific and the Atlantic. However, ICON-S simulates anomalous precipitation in the austral summer compared to the boreal summer over the equatorial Indian Ocean, even in the presence of a dry bias.

Tropical precipitation is also characterized by its specific diurnal cycle. Figure 1 c,d shows the mean diurnal cycle of precipitation in each grid cell averaged over the ocean and land, respectively. As in IMERG, ICON-S presents a peak in the early morning over the ocean. Over the land, ICON-S and IMERG show the expected late-afternoon strong diurnal peak, but differences exist. ICON-S shows a diurnal cycle with a precipitation peak of $\sim 0.37\,\mathrm{mm\,h^{-1}}$ occurring between 13 LT to 15 LT, twice more intense and two hours earlier than in IMERG. These types of discrepancies were not apparent in analyses of uncoupled ICON simulations using 0.6 km to 2.5 km grids over regional domains (Stevens et al., 2020). This suggests that either the yet coarser 5 km grid, or differences in the representation of non-convective processes may distort the development of the boundary layer over land, with consequences for the diurnal cycle as discussed by Petch et al. (2002). Another possibility is the remote effects of coupling to the ocean. However, the experiment presented in §6 leads us to rule out this possibility.

4 The ocean rainbelt

Using monthly mean precipitation from ICON-S and the monthly mean climatology of IMERG, we define a rainbelt by computing for each month the 80 % quantile of precipitation over the entire tropical ocean. After masking gridcells that fall below this value, we divide the tropical ocean in five regions, the tropical Atlantic, the eastern, central and southern Pacific and the Indian Ocean. In each region, we segment the remaining data and apply the SAL method to isolate the precipitation object with the maximum area. Only objects spanning a minimum area of $250\,000\,\mathrm{km^2}$ (roughly $5^\circ \times 5^\circ$) are retained and these are identified as the rainbelt of the respective ocean region. These form the basis for our further analysis of their structure (area) and location (centroid).

Figure 2 shows the seasonal movement and the change in the area of the rainbelt over the analyzed ocean regions. The agreement in the seasonal change of the location and the area of the rainbelt between ICON-S and IMERG is quantified by the correlation of the latitude (meridional migration), longitude (zonal migration) and area. In the five regions, the rainbelt possesses both a meridional and zonal migration, which ICON-S can reproduce, but with less agreement in the zonal movement. The correlation between ICON-S and IMERG are larger than 0.65 in in all regions regarding the meridional migration, while only the eastern Pacific and the Atlantic show correlation coefficients higher than 0.5 in the zonal migration. In details, ICON-S reproduces an opposite seasonal change in the zonal migration and a more poleward migration in the central Pacific. In the southern Pacific, ICON-S shows seven months in advance the most westward location of the rainbelt. And there is an anomalous eastward migration of the rainbelt in the Indian Ocean.

IMERG also indicates changes in the rainbelt extension in different ways across the different regions. The maximum area of the rainbelts in the Pacific coincides with their most poleward location, occurring in their respective summer seasons. The Atlantic has a different dynamic, with the maximum area occurring in the April-May season. All the above characteristics are reproduced by ICON-S with correlation coefficients higher than 0.71, with the Atlantic holding the highest correlation (r=0.84). In contrast, the low correlation value in the Indian Ocean is explained by the strongly seasonal areal change in the rainbelt simulated by ICON-S and not observed in IMERG. This is related to the splitting of the rainbelt displayed in Figure 1a.

In general ICON-S correctly represents a substantial component of the seasonal characteristic of the rainbelts, something models with parameterized convection struggle to do (Siongco et al., 2015; Wu et al., 2003). Nevertheless, ICON-S also has substantial precipitation biases in the Eastern Hemisphere. In this region the distorted representation of precipitation may be associated with substantial SST biases, the origin of which remain unclear. ICON-S simulates a cold-tongue that is both more pronounced and with a greater westward extension than in observations (Figure S2). Likewise the off equatorial SST are too warm in this region. To what extent this SST bias pattern impacts the representation of tropical precipitation is discussed further in §6.

5 The rainbelt over land

To analyze the rainbelt over tropical land, we use the same methodology as for the tropical ocean. We apply this analysis in four regions, South America, Africa, India and Southeast Asia. Figure 3 shows the seasonal migration and structural changes of the tropical rainbelt over land. In South America, the rainbelt reaches its southernmost (northernmost) position and shows its maximum extension during the austral (boreal) summer, the core of the monsoon (dry) season. As compared to over the ocean, ICON-S reproduces the seasonal behavior of the rainbelt in South America surprisingly well, with high correlation values in the latitude (0.98), longitude (0.93), and area (0.96).

The rainbelt in Africa shows similar characteristics as in South America in its North-South migration, which is restricted to a latitude band between 15°S and 15°N. In Africa, the largest area of the rainbelt occurs toward the end of boreal summer. ICON-S captures the meridional migration of the African rainbelt (r=0.99) but struggles in reproducing its seasonal areal changes. In particular, ICON-S does not reproduce the shrinking of the rainbelt in the May-July season, which explains the low correlation value (r=0.55) and the positive bias of precipitation over central Africa observed in Figure 1a. IMERG also identifies a pronounced east-west migration of more than 20°. ICON-S generally reproduces this feature, modulo one outlier point, which explains the slightly low correlation value of 0.74.

Over the South Asia subcontinent a large-scale ($>250\,000\,\mathrm{km}^2$) precipitation object is only observed from March to October for Southeast Asia and from June to October for India. Besides, both regions show a southward migration from the subtropics to 15°N. During its southward migration, the rainbelt over Southeast Asia expands, and its center of activity migrates from China to Myanmar, Thailand, and Laos. ICON-S reproduces the characteristics of the rainbelt in Southeast Asia, with correlation values in the latitude, longitude, and area of 0.97, 0.99, and 0.92, respectively. Over India, the SAL method can only capture the rainbelt in ICON-S for three months (July-September), indicating a dry onset and demise of the rainbelt compared to IMERG. Thus, from a tropical perspective, ICON-S with a grid spacing of 5 km reproduces the different characteristics of the rainbelt over land despite distortions of the diurnal cycle of precipitation.

6 Changing SST pattern

ICON-S has more difficulty in representing the structure and evolution of the tropical rainbelts over ocean than land, and this raises the question of the role of SST in explaining these difficulties. During the model development cycle, a similar simulation as ICON-S was performed in which the momentum transfer from the atmosphere to the ocean was switched off to test the influence of the wind-driven circulations on the simulations. This leads to substantial changes in the pattern of SST that allowed us to gain insights into the impact of the SST pattern on the tropical precipitation structure. In this experiment, the equatorial region over ocean is characterized by a strong warming compared to ICON-S, and for this reason, we named this experiment ICON-S_WarmEq. Because it was used to test ocean coupling it also uses a different vertical coordinate system in the ocean (Z_*) together with different parameterizations (See Table S1). It also covers a slightly different period, between January 20, 2020, and September 20, 2020.

Contrary to ICON-S, ICON-S_WarmEq produces an SST pattern with a less pronounced equatorial cold tongue (Figure 4 and Figure S2). The impact of this SST pattern is particularly evident in the Indian Ocean, where a single band of precipitation is reproduced in ICON-S_WarmEq (not shown) and where the rainbelt presents similar seasonal characteristic as seen in observation (r>0.6 in Figure 4). Moreover, the SST pattern in ICON-S_WarmEq is related to a wet onset and demise of the Indian monsoon (Figure S3). In the other ocean regions, correlation values between ICON-S_WarmEq vs. IMERG and ICON-S vs. IMERG are similar (Figures 2 and 4), but the limits in the meridional migration changes. It is interesting that the rainbelt over the central Pacific is constrained in its poleward migration, when the cold bias at the equator is not simulated (Figure S2). This analysis points to SST biases as the explanation for the misrepresentation of the tropical rainbelts by ICON-S in the Eastern Hemisphere. As expected changes in SSTs do not impact the diurnal cycle of precipitation (Figure 1c,d). Whether the biases in the SSTs are caused by distortions in the convection that arise from the relatively coarse (5 km) resolution, or errors in the representation of other processes remains unclear, but short simulations at finer resolution suggest that the latter is more likely.

7 Conclusions

In this study, we explore the representation of the seasonal and diurnal features of tropical precipitation in a new configuration of ICON (ICON-S), which couples ocean, land and atmospheric processes on a 5 km-scale global grid. Our objective was to assess the capabilities of this configuration in representing the observed response of precipitation to annual and diurnal forcing.

ICON-S reproduces the seasonal migration and areal change of the tropical rainbelts over land with surprising fidelity, surpassing the statistics over the ocean. Aside from capturing the North-South and East-West migration of the terrestrial rainbelts, their enlargement during the monsoon season is also represented – correlations with observations vary between 0.55 and 0.9. The fidelity of the annual cycle is apparent despite some distortion in the representation of the diurnal cycle, where the convection couples too strongly to forcing. Although generally improved as compared to what is found with parameterized convection, the diurnal cycle is stronger than observed, and peaks too early. Hence, a perfect representation of the diurnal cycle of precipitation is not a primary requirement for a correct representation of the seasonal precipitation variability over land.

ICON-S also reproduces the seasonal characteristics of the rainbelts over ocean, but with less agreement in the zonal migration, especially over the Eastern Hemisphere. Except over the Indian ocean, the North-South migration is reproduced by ICON-S with correlation values higher than 0.66, and the change in area with values larger than 0.71. The poor representation of the rainbelt in the Indian Ocean and the anomalous northward migration of the rainbelt in the central Pacific is shown to arise from cold SST biases at the equator. Moreover, warming the SSTs over the equatorial Indo-Pacific region, to be in better agreement with the observations, increases precipitation during the onset and demise of the monsoon season in the Indian continent.

Our analysis identifies challenges and opportunities in the development of coupled GSRMs for climate applications. It demonstrates an ability of such models to represent the basic response of precipitation to diurnal forcing over ocean and land. The diurnal cycle over land, while too strong, and still too early neither evinces a sensitivity to the large-scale circulation, nor does it seem coupled to the ability of the simulations to represent the response to annual cycle of forcing over land. The migration of the ITCZ is well captured over many ocean basins, particularly in the Western Hemisphere. Over the Indian and Western Pacific Oceans the distribution of convection is sensitive to errors in the SST along the equator. Whether these errors are due to the representation of convection itself, a poor representation of other processes, or simply errors reflecting the early stage of development of the model remains to be understood, but should guide future work. This points to the fact that GSRMs are not only tools for better climate projections, but efforts to identify the causes of their remaining biases provides new opportunities to understand the Earth System.

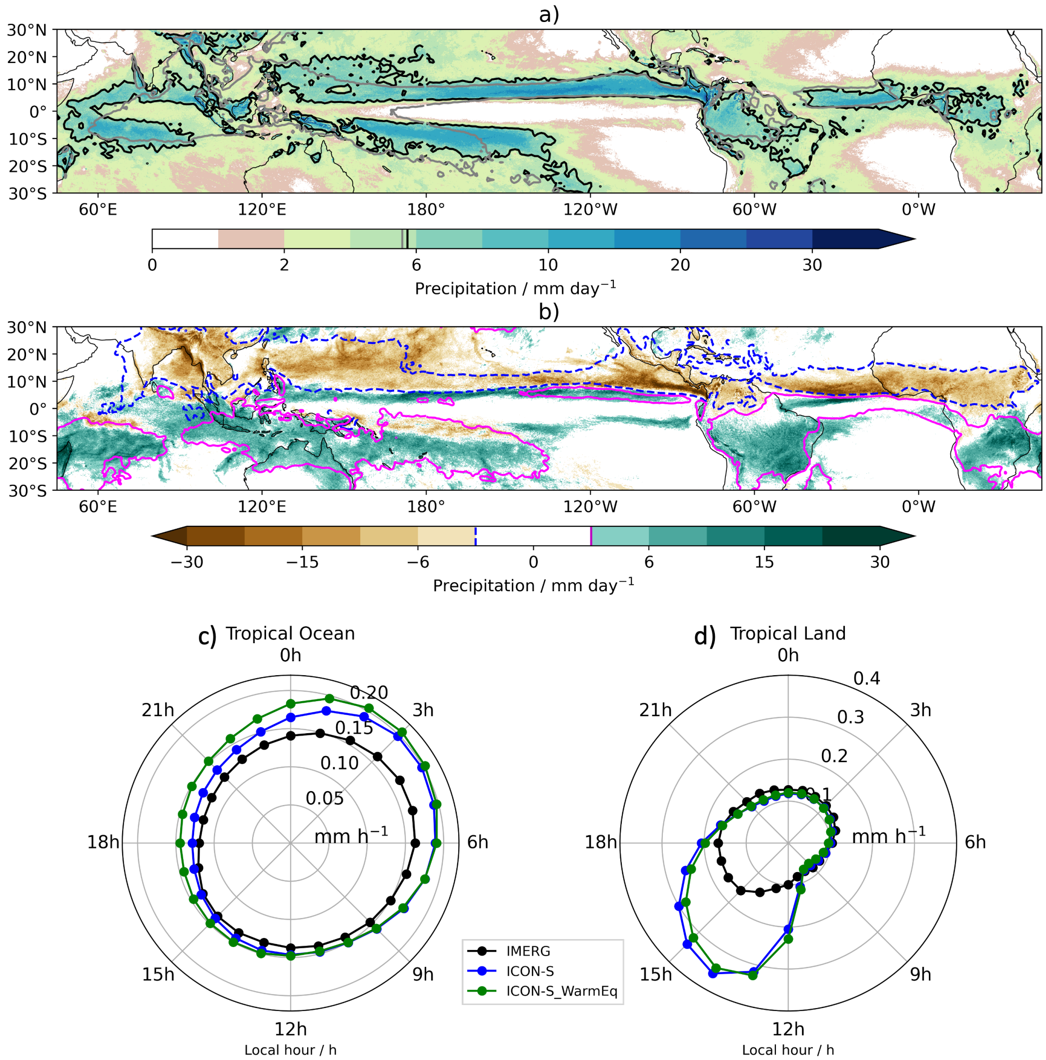

Figure 1. a) Annual mean precipitation in ICON-S (January 2020 – February 2021; shaded). The quantile 80 of the annual mean of both ICON-S (black contour) and the climatology of IMERG (2001-2020; gray contour) are shown. b) January–February 2021 minus August–September 2020 precipitation in ICON-S (shaded). In IMERG, the climatology of both seasons is used and only the contour lines of $3\,\mathrm{mm\,d^{-1}}$ (magenta) and $-3\,\mathrm{mm\,d^{-1}}$ (blue) are plotted. In a,b), the values of the contours are indicated in the colorbar. c,d) Clock diagram of the diurnal cycle of precipitation over the tropical ocean and the tropical land, respectively, for February 2020. The angles represent the local hour and the radius the intensity. IMERG, ICON-S, and ICON-S_WarmEq are represented by a black, blue, and green line, respectively.

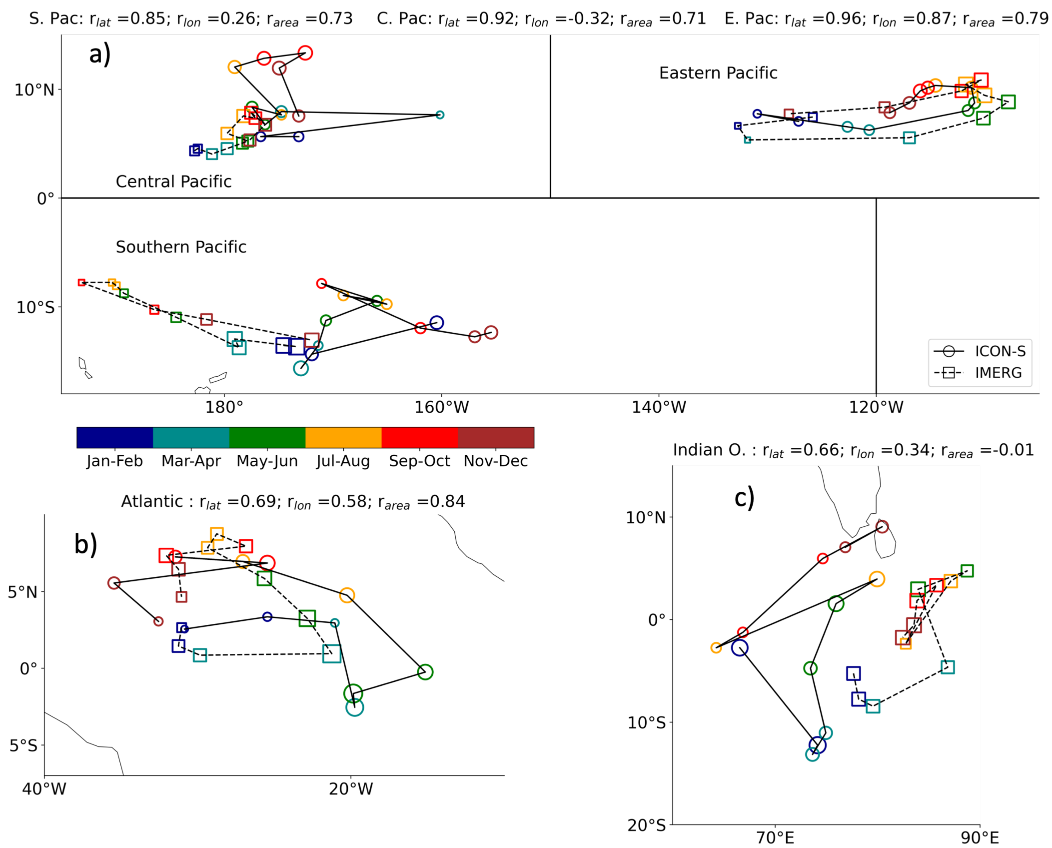

Figure 2. Monthly mean location of the centroid of the rainbelt over the tropical ocean calculated by using the SAL method from ICON-S (circles and solid lines) and IMERG (squares and dashed lines). Marker colors indicate the month and for a better visualization, colors are grouped by two months. Marker size represents the ratio between the area of the rainbelt in each month compared to the annual mean. a) the eastern Pacific (0°N-20°N;150°W-80°W), the central Pacific (0°N-20°N;160°E-150°W), the Southern Pacific (20°S-0°N;160°E-150°W), b) the Atlantic Ocean (60°W-10°E;10°S-20°N), c) the Indian Ocean (50°E-105°E;30°S-30°N). The correlation values between ICON-S and IMERG for the longitude and latitude of the centroid and its area are shown in the upper part of each subplot.

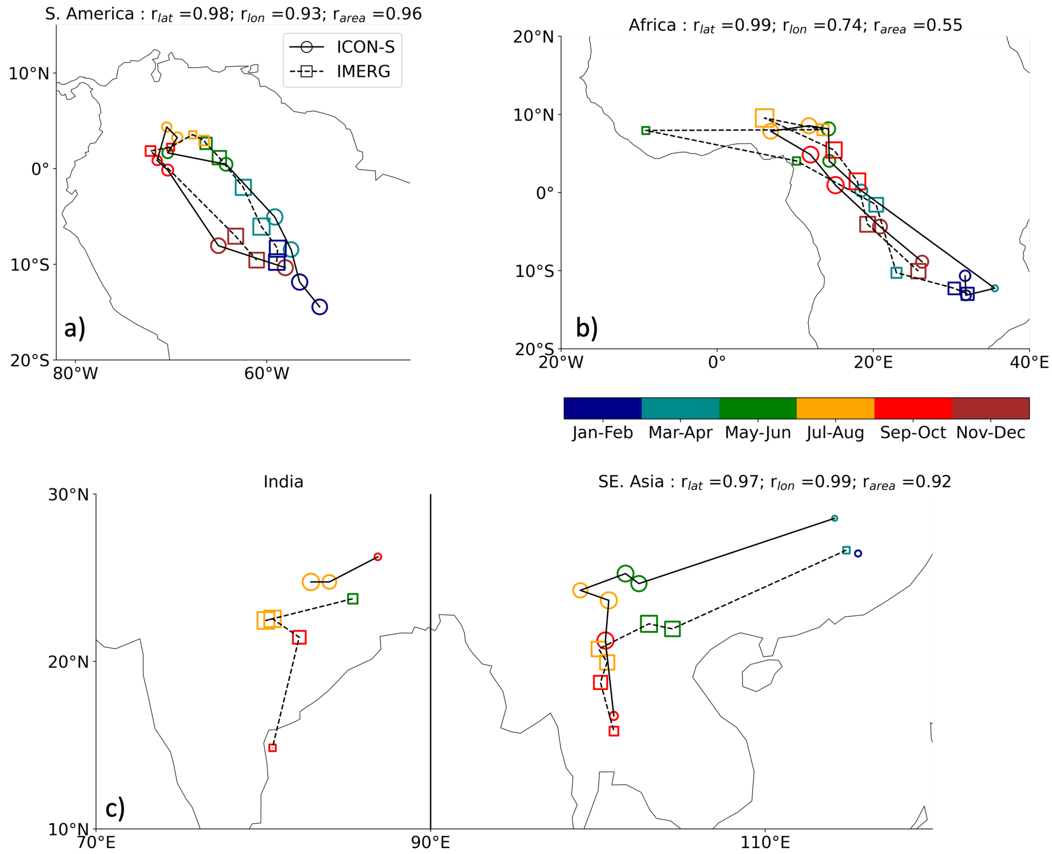

Figure 3. Similar to Fig. 2, but only over the tropical land. a) South America (82°W-30°W;30°S-13°N), b) Africa (20°W-45°E;30°S-25°N), and c) India (70°E-90°E;10°N-30°N) and Southeast Asia (90°E-120°E;10°N-30°N).

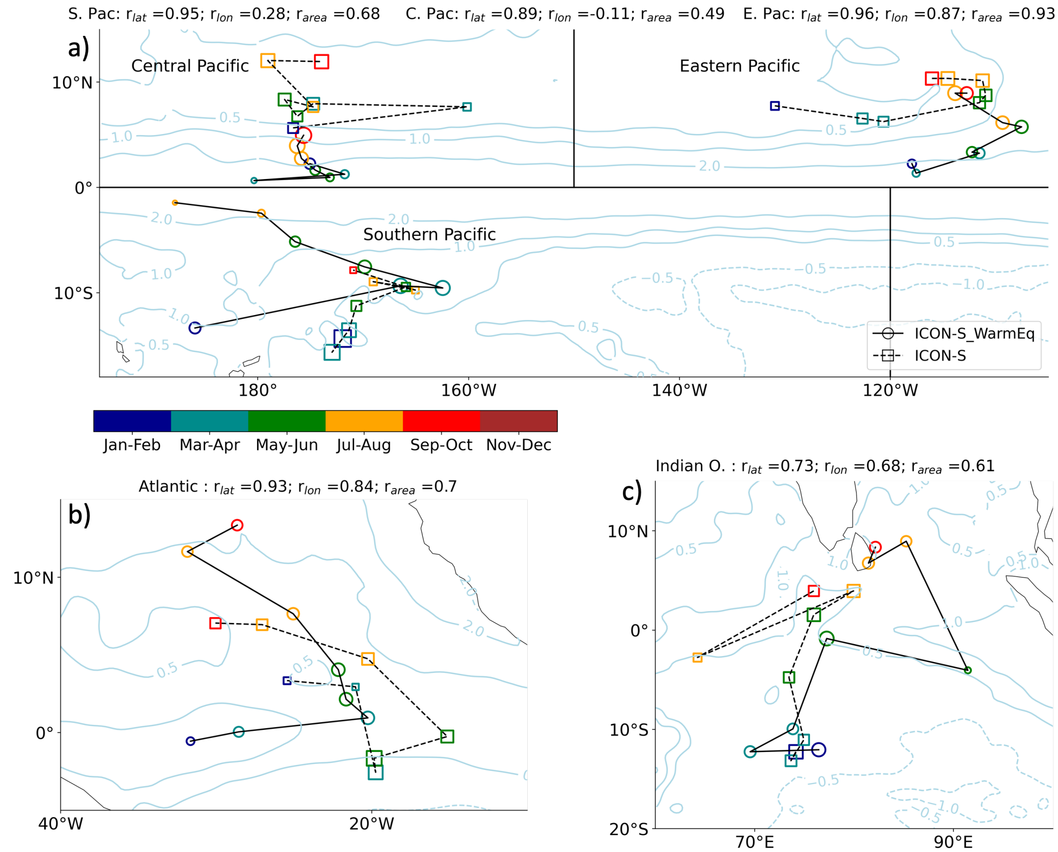

Figure 4. a-c) Similar to Fig. 2, but using ICON-S_WarmEq and ICON-S and between February 1 to September 22, 2020. The sea surface temperature (SST) difference between ICON-S_WarmEq and ICON-S is shown. Positive (negative) values are plotted in solid (dashed) contours and the contour line of 0 K is omitted. SST is interpolated to a resolution of 0.25°. The correlation values in the upper part of each panel are calculated between IMERG and ICON-S_WarmEq.

8 Open Research

The ICON-S simulation were done with the ICON branch nextgems_cycle1_dpp0066 as commit 62dbfc. And the ICON-S_WarmEq were done with the ICON branch nextgems_cycle1_zstar as commit 32adb2, 83f3dc, c17dcc. The source code is available here `https://doi.org/10.17617/3.1XTSR6`. The ICON model is available to individuals under licenses (`https://mpimet.mpg.de/en/science/modeling-with-icon/code-availability`). The IMERG data was obtained from `https://www.cen.uni-hamburg.de/en/icdc/data/atmosphere/imerg-precipitation-amount.html` and the HadISST data from `https://www.cen.uni-hamburg.de/en/icdc/data/ocean/hadisst1.html`. The scripts used to process the data and to plot the figures in the paper can be found in the git repository: `https://gitlab.gwdg.de/hans.segura/tropical_precipitation.git`

Acknowledgments

H. Segura received funding from the Hans-Ertel Centre for Weather Research under project number 4818DWDP1A. The European Union's Horizon 2020 research and innovation program project NextGEMS funded C. Hohenegger and B.Stevens under the grant agreement number 101003470. The European Horizon 2020 project CONSTRAIN, project number 493B, is acknowledged by the authors. The authors also acknowledge the DKRZ compute time, project bm1235 and bb1153. We thank to Lukas Kluft for his comments on the final version of the manuscript.

References

Adam, O., Bischoff, T., & Schneider, T. (2016). Seasonal and interannual variations of the energy flux equator and ITCZ. Part I: Zonally averaged ITCZ position. *J. Clim.*, *29*(9), 3219–3230. doi: 10.1175/JCLI-D-15-0512.1

Baldauf, M., Seifert, A., Förstner, J., Majewski, D., Raschendorfer, M., & Reinhardt, T. (2011). Operational convective-scale numerical weather prediction with the COSMO model: Description and sensitivities. *Mon. Weather Rev.*, *139*(12), 3887–3905. doi: 10.1175/MWR-D-10-05013.1

Bulovic, N., McIntyre, N., & Johnson, F. (2020). Evaluation of imerg v05b 30-min rainfall estimates over the high-elevation tropical andes mountains. *J. Hydrometeorol.*, *21*(12), 2875–2892. doi: 10.1175/JHM-D-20-0114.1

Dirmeyer, P. A., Cash, B. A., Kinter, J. L., Jung, T., Marx, L., Satoh, M., ... Manganello, J. (2012). Simulating the diurnal cycle of rainfall in global climate models: Resolution versus parameterization. *Clim. Dyn.*, *39*(1-2), 399–418. doi: 10.1007/s00382-011-1127-9

Done, J., Davis, C. A., & Weisman, M. (2004). The next generation of NWP: Explicit forecasts of convection using the weather research and forecasting (WRF) model. *Atmos. Sci. Lett.*, *5*(6), 110–117. doi: 10.1002/asl.72

Fiedler, S., Crueger, T., D'Agostino, R., Peters, K., Becker, T., Leutwyler, D., ... Stevens, B. (2020). Simulated tropical precipitation assessed across three major phases of the coupled model intercomparison project (CMIP). *Mon. Weather Rev.*, *148*(9), 3653–3680. doi: 10.1175/MWR-D-19-0404.1

Gassmann, A. (2013). A global hexagonal C-grid non-hydrostatic dynamical core (ICON-IAP) designed for energetic consistency. *Q. J. R. Meteorol. Soc.*, *139*(670), 152–175. doi: 10.1002/qj.1960

Grell, G. A., Schade, L., Knoche, R., Pfeiffer, A., & Egger, J. (2000, dec). Nonhydrostatic climate simulations of precipitation over complex terrain. *J. Geophys. Res. Atmos.*, *105*(D24), 29595–29608. Retrieved from `https://doi.org/10.1029/2000JD900445` doi: https://doi.org/10.1029/2000JD900445

Hohenegger, C., Brockhaus, P., & Schär, C. (2008). Towards climate simulations at cloud-resolving scales. *Meteorol. Zeitschrift*, *17*(4), 383–394. doi: 10.1127/0941-2948/2008/0303

Hohenegger, C., Korn, P., Linardakis, L., Redler, R., Schnur, R., Adamidis, P., … Stevens, B. (2022). ICON-Sapphire: simulating the components of the Earth System and their interactions at kilometer and sub-kilometer scales. *Geosci. Model Dev. Discuss.*, *2022*, 1–42. Retrieved from https://gmd.copernicus.org/preprints/gmd-2022-171/ doi: 10.5194/gmd-2022-171

Hohenegger, C., & Stevens, B. (2013). Controls on and impacts of the diurnal cycle of deep convective precipitation. *J. Adv. Model. Earth Syst.*, *5*(4), 801–815. doi: 10.1002/2012ms000216

Hohenegger, C., & Stevens, B. (2022, aug). Tropical Continents Rainier Than Expected From Geometrical Constraints. *AGU Adv.*, *3*(4), e2021AV000636. Retrieved from https://doi.org/10.1029/2021AV000636 doi: https://doi.org/10.1029/2021AV000636

Huffman, G., Stocker, E., Bolvin, D., Nelkin, E., & Tan, J. (2019). *GPM IMERG Final Precipitation L3 Half Hourly 0.1 degree x 0.1 degree V06* (Tech. Rep.). Greenbelt, MD, Goddard Earth Sciences Data and Information Services Center (GES DISC),[last access: February 26, 2022], distributed in netCDF file format by ICDC, CEN, University of Hamburg. doi: 10.5067/GPM/IMERG/3B-HH/06

Lu, D., & Yong, B. (2018). Evaluation and hydrological utility of the latest GPM IMERG V5 and GSMaP V7 precipitation products over the Tibetan Plateau. *Remote Sens.*, *10*(12). doi: 10.3390/rs10122022

Marsham, J. H., Dixon, N. S., Garcia-Carreras, L., Lister, G. M., Parker, D. J., Knippertz, P., & Birch, C. E. (2013). The role of moist convection in the West African monsoon system: Insights from continental-scale convection-permitting simulations. *Geophys. Res. Lett.*, *40*(9), 1843–1849. doi: 10.1002/grl.50347

Mellado, J. P., Bretherton, C. S., Stevens, B., & Wyant, M. C. (2018). DNS and LES for Simulating Stratocumulus: Better Together. *J. Adv. Model. Earth Syst.*, *10*(7), 1421–1438. doi: 10.1029/2018MS001312

Miura, H., Satoh, M., Nasuno, T., Akira, T., N., & Oouchi, K. (2007, dec). A Madden-Julian Oscillation Event Realistically Simulated by a Global Cloud-Resolving Model. *Science (80-.).*, *318*(5857), 1763–1765. Retrieved from https://doi.org/10.1126/science.1148443 doi: 10.1126/science.1148443

Miura, H., Satoh, M., Tomita, H., Noda, A. T., Nasuno, T., & Iga, S. I. (2007). A short-duration global cloud-resolving simulation with a realistic land and sea distribution. *Geophys. Res. Lett.*, *34*(2), 2–6. doi: 10.1029/2006GL027448

Pearson, K. J., Lister, G. M., Birch, C. E., Allan, R. P., Hogan, R. J., & Woolnough, S. J. (2014). Modelling the diurnal cycle of tropical convection across the 'grey zone'. *Q. J. R. Meteorol. Soc.*, *140*(679), 491–499. doi: 10.1002/qj.2145

Petch, J. C., Brown, A. R., & Gray, M. E. (2002). The impact of horizontal resolution on the simulations of convective development over land. *Q. J. R. Meteorol. Soc.*, *128*(584 PART B), 2031–2044. doi: 10.1256/003590002320603511

Pfeifroth, U., Mueller, R., & Ahrens, B. (2013). Evaluation of satellite-based and reanalysis precipitation data in the tropical pacific. *J. Appl. Meteorol. Climatol.*, *52*(3), 634–644. doi: 10.1175/JAMC-D-12-049.1

Prein, A. F., Gobiet, A., Suklitsch, M., Truhetz, H., Awan, N. K., Keuler, K., & Georgievski, G. (2013). Added value of convection permitting seasonal simulations. *Clim. Dyn.*, *41*(9-10), 2655–2677. doi: 10.1007/s00382-013-1744-6

Samanta, D., Karnauskas, K. B., & Goodkin, N. F. (2019). Tropical Pacific SST and ITCZ Biases in Climate Models: Double Trouble for Future Rainfall Projections? *Geophys. Res. Lett.*, *46*(4), 2242–2252. doi: 10.1029/2018GL081363

Satoh, M., Stevens, B., Judt, F., Khairoutdinov, M., Lin, S.-J., Putman, W. M., & Düben, P. (2019). Global Cloud-Resolving Models. *Curr. Clim. Chang. Reports*, *5*(3), 172–184. Retrieved from https://doi.org/10.1007/s40641-019-00131-0 doi: 10.1007/s40641-019-00131-0

Satoh, M., Tomita, H., Yashiro, H., Kajikawa, Y., Miyamoto, Y., Yamaura, T., ... Fukutomi, Y. (2017). Outcomes and challenges of global high-resolution non-hydrostatic atmospheric simulations using the K computer. *Prog. Earth Planet. Sci.*, *4*(1). doi: 10.1186/s40645-017-0127-8

Schär, C., Fuhrer, O., Arteaga, A., Ban, N., Charpilloz, C., Di Girolamo, S., ... Wernli, H. (2020). Kilometer-Scale Climate Models: Prospects and Challenges. *Bull. Am. Meteorol. Soc.*, *101*(5), E567–E587. Retrieved from `https://journals.ametsoc.org/view/journals/bams/101/5/bams-d-18-0167.1.xml` doi: 10.1175/BAMS-D-18-0167.1

Schneider, T., Bischoff, T., & Haug, G. H. (2014). Migrations and dynamics of the intertropical convergence zone. *Nature*, *513*(7516), 45–53. Retrieved from `http://www.nature.com/doifinder/10.1038/nature13636` doi: 10.1038/nature13636

Siongco, A. C., Hohenegger, C., & Stevens, B. (2015). The Atlantic ITCZ bias in CMIP5 models. *Clim. Dyn.*, *45*(5-6), 1169–1180. Retrieved from `http://dx.doi.org/10.1007/s00382-014-2366-3` doi: 10.1007/s00382-014-2366-3

Siongco, A. C., Hohenegger, C., & Stevens, B. (2017). Sensitivity of the summertime tropical Atlantic precipitation distribution to convective parameterization andmodel resolution in ECHAM6. *J. Geophys. Res.*, *122*(5), 2579–2594. doi: 10.1002/2016JD026093

Slingo, J., Bates, P., Bauer, P., Belcher, S., Palmer, T., Stephens, G., ... Teutsch, G. (2022). Ambitious partnership needed for reliable climate prediction. *Nat. Clim. Chang.*, *12*(6), 499–503. Retrieved from `https://doi.org/10.1038/s41558-022-01384-8` doi: 10.1038/s41558-022-01384-8

Stevens, B., Acquistapace, C., Hansen, A., Heinze, R., Klinger, C., Klocke, D., ... Zängl, G. (2020). The added value of large-eddy and storm-resolving models for simulating clouds and precipitation. *J. Meteorol. Soc. Japan*, *98*(2), 395–435. doi: 10.2151/jmsj.2020-021

Stevens, B., Moeng, C. H., & Sullivan, P. P. (1999). Large-eddy simulations of radiatively driven convection: Sensitivities to the representation of small scales. *J. Atmos. Sci.*, *56*(23), 3963–3984. doi: 10.1175/1520-0469(1999)056⟨3963:LESORD⟩2.0.CO;2

Wernli, H., Paulat, M., Hagen, M., & Frei, C. (2008). SAL - A novel quality measure for the verification of quantitative precipitation forecasts. *Mon. Weather Rev.*, *136*(11), 4470–4487. doi: 10.1175/2008MWR2415.1

Wu, X., Liang, X. Z., & Zhang, G. J. (2003). Seasonal migration of ITCZ precipitation across the equator: Why can't GCMs simulate it? *Geophys. Res. Lett.*, *30*(15), 10–13. doi: 10.1029/2003GL017198

Learning by doing: seasonal and diurnal features of tropical precipitation in a global-coupled storm-resolving model

H. Segura[1], C. Hohenegger[1], C. Wengel[1], B. Stevens[1]

[1]Max-Planck-Institute for Meteorology, Hamburg, Germany

Contents of this file

Figure S1

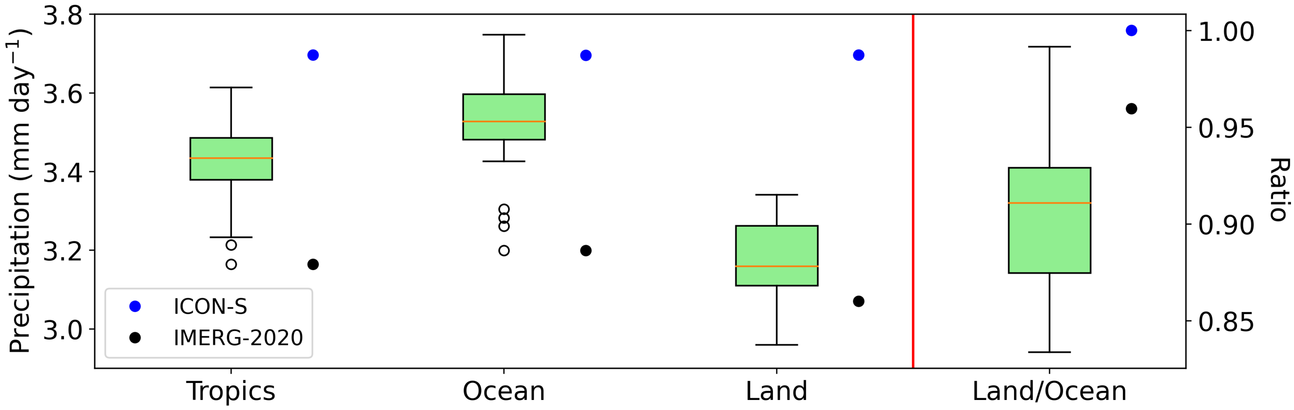

Figure S1. To the left of the vertical red line: box plot of the annual mean values of precipitation in the tropics (Tropics), tropical ocean (Ocean), and tropical land (Land) using IMERG from January 2001 to December 2020. The annual mean of precipitation in ICON-S and IMERG in 2020 (IMERG-2020) is plotted as a blue and black circle, respectively, to the right of each box. For ICON-S and IMERG-2020, the annual mean value is calculated using data from February 2020 to January 2021. To the right of the vertical red line: box plot of the annual mean precipitation ratio between land and ocean in the tropics (Land/Ocean) in IMERG. The ratio is calculated for each year between January 2001 to December 2020. The ratio in ICON-S and IMERG-2020 is shown as a blue and black circle, respectively, to the right of the box. The ratio in ICON-S and IMERG-2020 is calculated using the annual mean precipitation between February 2020 to January 2021

Figure S2

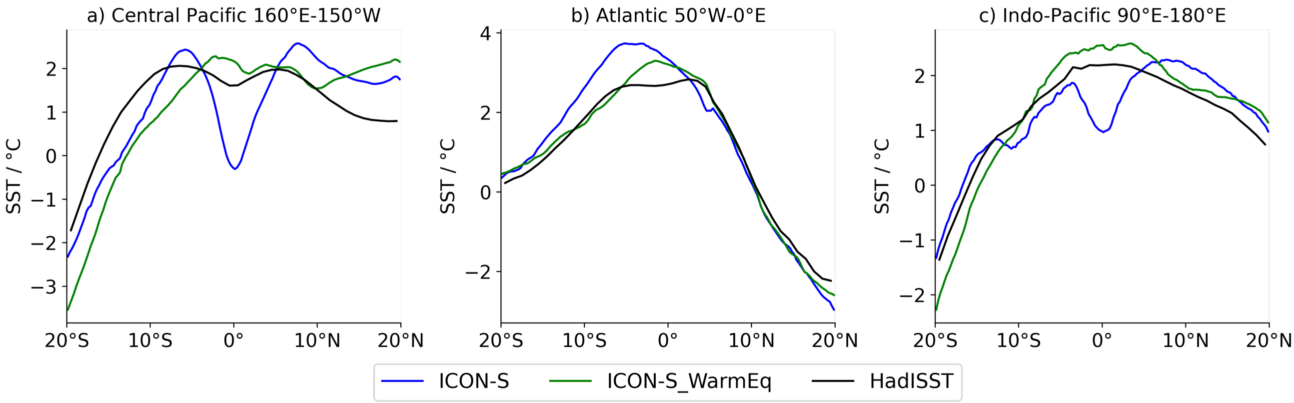

Figure S2. Zonal-mean sea surface temperature anomalies (SST) using ICON-S (blue line), ICON-S_WarmEq (green line) and the climatology of the HadISST data (black line, 2001-2020) in: a) the central Pacific, b) the Atlantic and c) the Indo-Pacific. The anomalies are calculated by subtracting the mean of each region between 30°S-30°N . In a),b), c) the zonal-mean is calculated from June to September 2020, from March to May 2020, and from February to September 2020, respectively, for ICON-S and ICON-S_WarmEq. In both simulations SST is interpolated to a resolution of 0.25°. For HadISST, the zonal-mean is computed using the climatology of the months used for ICON-S.

Figure S3

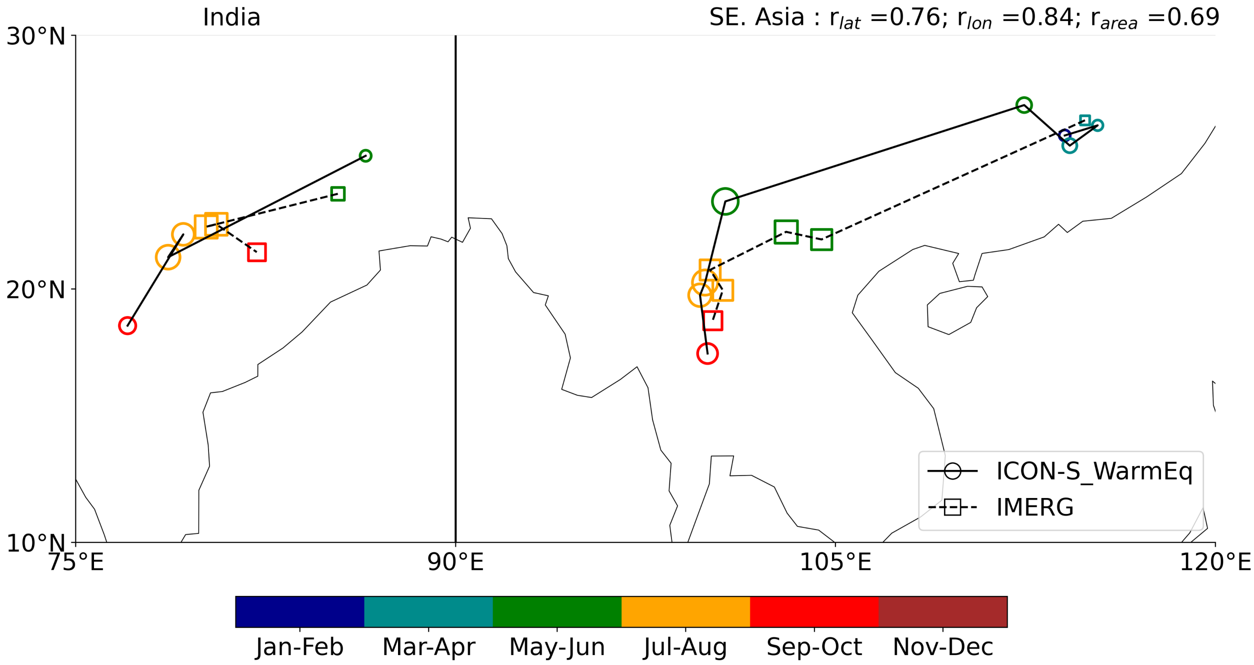

Figure S3. Location of the centroid of the rainbelt over India (70°E-90°E;10°N-30°N) and Southeast Asia (90°E-120°E;10°N-30°N) calculated by using the SAL method and monthly mean precipitation values from ICON-S_WarmEq (circles) and IMERG (squares). Circles are connected by a solid line, while squares are by a dashed line. The color of the edge of the markers indicates the month used to calculate the centroid (from January to December) and for a better visualization, colors are grouped by two months. The size of the markers represents the ratio between the area of the precipitation structure in each month and the annual mean area, calculated for ICON-S_WarmEq and IMERG, separately. The correlation values between the longitude and the latitude of the centroids between ICON-S_WarmEq and IMERG, as well as the correlation between the areas of the precipitation structures, are shown in the upper part of the plot only for Southeast Asia.

Table S1. Ocean configuration in ICON-S and ICON-S_WarmEq

Simulation	Vertical coordinate	First layer depth	TKE coefficient	Jerlov scheme	Viscosity
ICON-S	Z	7 meters	0.3	la	Leith
ICON-S_WarmEq	Z*	2 meters	0.1	lb	Biharmonic

[a] Footnote text here.